Materials Horizons

ROYAL SOCIETY OF CHEMISTRY

COMMUNICATION

View Article Online
View Journal | View Issue

Cite this: *Mater. Horiz.*, 2025, 12, 987

Received 27th July 2024,
Accepted 7th November 2024

DOI: 10.1039/d4mh00981a

rsc.li/materials-horizons

Targeted and precise drug delivery using a glutathione-responsive ultra-short peptide-based injectable hydrogel as a breast cancer cure†

Satyajit Halder,[a] Tanushree Das,[b] Ritvika Kushwaha,[b] Anup Kumar Misra,[a] Kuladip Jana *[a] and Debapratim Das *[b]

Harnessing the potential of hydrogel-based localized drug delivery systems holds immense promise for mitigating the systemic side effects associated with conventional cancer therapies. However, the development of such systems demands the fulfillment of multiple stringent criteria, including injectability, biocompatibility, and controlled release. Herein, we present an ultra-small peptide-based hydrogel for the sustained and targeted delivery of doxorubicin in a murine model of breast cancer. The hydrogel evades dissolution and remains stable in biological fluids, serving as a reliable drug reservoir. However, it specifically reacts to the high levels of glutathione (GSH) in the tumor microenvironment and releases drugs in a controlled manner over time for consistent therapeutic benefits. Remarkably, administration of a single dose of doxorubicin-loaded hydrogel elicited superior tumor regression (approximately 75% within 18 days) compared to conventional doxorubicin treatment alone. Furthermore, the persistent presence of the drug-loaded hydrogel near the tumor site for up to 18 days after administration highlights its enduring effectiveness. There is great clinical potential for this localized delivery strategy because of the minimal off-target effects on healthy tissues. Our findings underscore the efficacy of this smart peptide-hydrogel platform and pave the way for developing next-generation localized drug delivery systems with enhanced therapeutic outcomes in cancer treatment.

New concepts

Although supramolecular hydrogels have been considered as drug delivery vehicles, their use has been restricted to topical or transdermal applications. To apply them to localized delivery, it is necessary for the hydrogels to demonstrate injectability, respond to particular stimuli present near the tumor, and remain insoluble in the biofluid. Unfortunately, no such supramolecular hydrogel has thus far been reported that fulfils these criteria. Herein, we have reported an ultra-short peptide-based hydrogel that satisfies these essential requirements. The injectable hydrogel is insoluble in blood serum and responsive to the excess glutathione present near the tumor. Loaded with a drug, when injected onto a breast tumor, sustained and efficient release of the drug occurred that effectively reduced the tumor by approximately 75% within 18 days after a single injection and with no detectable side effects. This new hydrogel can pave the way for a new method of cancer treatment in the future.

Introduction

Cancer is a global threat to mankind. Over the years, a significant understanding of the cause, behavior, and drugs required to cure various cancers has accumulated.[1,2] However, the therapeutic procedures for cancer remain a major concern for scientists. Depending upon the type or location, cancers can be treated through medicines or surgical resection/amputation.[2–5] However, the recurrence rate of tumors is high after surgery, and chemotherapy is the main treatment against tumor recurrence.[4,6–8] Moreover, surgical processes are not applicable for many internal organs or tissues because amputation of malignant organs may lead to severe post-surgical problems.[4,9]

Oral or intravenous drug intakes are not effective in many cases unless the formulation consists of a targeted delivery vehicle.[10–14] Even with the incorporation of targeting groups, there are several disadvantages for these systems when the vehicle is intravenously introduced, including loss of drugs leading to excess use of the drug, and dilution factor.[10,11,15,16] Moreover, interaction with healthy cells cannot be completely prevented because the blood flows throughout the body, and the anti-cancer drug passes through every organ and tissue. In this regard, local administration of the formulation (localized

[a] *Division of Molecular Medicine, Bose Institute, P 1/12, CIT Scheme VIIM, Kolkata – 700 054 and Unified Academic Campus, EN 80, Sector V, Salt Lake City, Bidhan Nagar, Kolkata 700091, India. E-mail: kuladip@jcbose.ac.in*

[b] *Department of Chemistry, Indian Institute of Technology Guwahati, North Guwahati, Assam 781039, India. E-mail: ddas@iitg.ac.in*

† Electronic supplementary information (ESI) available: Contains a detailed Experimental section and other related supporting data, figures, and tables. See DOI: https://doi.org/10.1039/d4mh00981a

drug delivery system (LDDS)) is a much more attractive method of treatment, and several experimental systems have been implemented thus far.[17,18] Most of these systems are solution-based and use various types of carriers. Because these systems are solution-based, the drug-loaded vehicles eventually mix with the bloodstream, leading to the above-mentioned issues of side effects and loss of drug.[19] Thus, LDDSs are primarily restricted to topical and subcutaneous applications.[20–22]

Hydrogel-based systems appear to be a more effective alternative to overcome these problems. For a hydrogel-based drug delivery system, it is understandable that the gel cannot be intravenously administered. Except for topical or transdermal applications, localized application of a drug-loaded hydrogel on an internal tumor is the only way to use these systems.[23] For the localized sustained release of drugs, the hydrogel should: (a) be injectable (shear thinning); (b) not be highly soluble in bio-fluid because it may wash out after administration; (c) be biocompatible; (d) release the payload in response to the stimuli that is overproduced/expressed at the tumor site.[21,23,24]

Creating systems that fulfill all these criteria is an uphill task. Over the last few decades, many efforts have been made to create hydrogel-based delivery vehicles. However, the majority of them are based on polymeric materials.[24,25] On many occasions, synthetic polymeric systems require modification due to their bio-incompatibility or non-degradability.[26] In this regard, supramolecular gels, especially from small peptides, are attractive alternatives.[27,28] Peptide-based hydrogels are prepared from natural amino acids, and it has been determined that they are biocompatible and easily degradable. However, most of these hydrogels do not satisfy some or all of the above-mentioned criteria.

Recently, we reported an ultrasmall peptide-based hydrogel (PyKC, Fig. 1a) that, unlike other supramolecular hydrogels, remained insoluble in water and human blood serum (HBS) even after incubation for more than a year.[29–34] The PyKC-hydrogel is produced *via* dimerization of PyKC peptides through disulfide linkages under neutral to basic conditions. The PyKC dimers self-assemble to form a tightly knitted network where water molecules get trapped through cohesive forces. Thus, the hydrogel is responsive to disulfide bond-breaking agents such as TCEP, DDT, and, most importantly, glutathione (GSH). GSH is important in many cellular processes, including cell differentiation, proliferation, and apoptosis. Disturbances in GSH homeostasis are involved in the etiology and progression of many human diseases, including cancer.

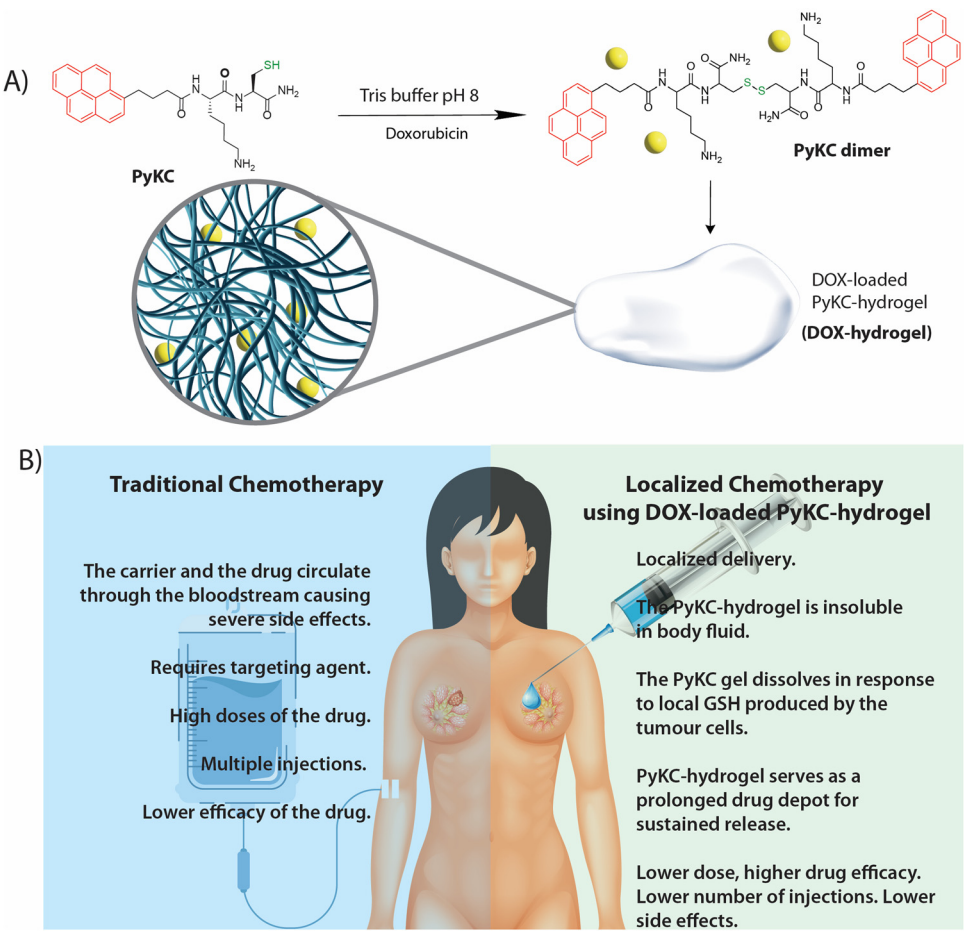

Fig. 1 (a) Hydrogelation by PyKC while entrapping DOX in the gel matrix. (b) Comparative analyses of traditional chemotherapy and the PyKC-hydrogel-based localized delivery system.

Importantly, elevated GSH levels are observed in various types of tumors, including cancerous ones, which results in the neoplastic tissues becoming more resistant to chemotherapy.[35,36] Thus, GSH-responsive systems could be an excellent choice for drug delivery.

In the case of the PyKC-hydrogel, in addition to its GSH responsiveness and insolubility in HBS, it also showed extreme confinement properties. The hydrogel does not allow any movement of any solute or solvent to or from the hydrogel network. We have also reported the thixotropic behavior of the hydrogel that allows it to be easily injected from a syringe.[37] Because of these properties, the PyKC-hydrogel is a perfect candidate to test for determination of its efficiency as a localized drug delivery system.

In this work, we demonstrated the use of a drug-loaded PyKC-hydrogel as a localized drug delivery system to treat breast cancer in a mouse model. Sustained release of the drug in response to the local GSH concentration was achieved. Thus, a single injection of the doxorubicin (DOX)-loaded PyKC-hydrogel resulted in significant reduction of the tumor. Even after 18 days, the hydrogel and DOX were present near the tumor, demonstrating effective slow and sustained release. Notably, the PyKC-hydrogel provided an alternative method to treat breast cancer and overcome many of the shortcomings of traditional chemotherapy, as shown in Fig. 1b.

Results and discussion

Injectability, insolubility, and GSH-responsive DOX release

The PyKC peptide was prepared using a modified solution-based peptide synthesis method, as described in the ESI.† The hydrogel of the peptide was prepared by dissolving the appropriate amount of freeze-dried PyKC in 20 mM phosphate-buffered saline (PBS) buffer, pH 7.4. For complete dimerization of the PyKC peptide to form $(PyKC)_2$ and subsequent gelation, 12 h are required. However, to ensure proper gelation, all samples were incubated at room temperature for 24 h before use. As mentioned in the introduction, one of the primary requirements for the use of hydrogel as a localized delivery system is that it must be injectable. In our previous work, we demonstrated the injectable property of the PyKC-hydrogel.[37] However, the loading of DOX in the hydrogel (DOX-hydrogel) may affect its rheological properties, and thus, a detailed rheological investigation on DOX-hydrogel was performed and compared with that of PyKC-hydrogel.

Studies using DOX-hydrogels were performed with a maximum concentration of 2.5 mM DOX, and therefore, the effect of the presence of DOX in the hydrogel matrix was studied using this particular concentration of DOX (DOX (2.5 mM)-hydrogel). The transmission electron microscopy (TEM) analyses of the PyKC-hydrogel and the DOX-loaded PyKC-hydrogel did not show any morphological changes (Fig. S1, ESI†). The hydrogel with and without DOX was subjected to amplitude sweep and frequency sweep experiments (Fig. 2a and b). In both cases, the storage modulus (G') was found to be higher than the loss modulus (G''), indicating the gel state. Although the presence of DOX in the hydrogel resulted in a slight weakening of the hydrogel (Fig. 2a and b), the system maintained the gel state as G' remained higher than G''.

To assess the injectability of the hydrogels, cyclic strain-time sweep experiments (Fig. 2c) were conducted on both hydrogels.

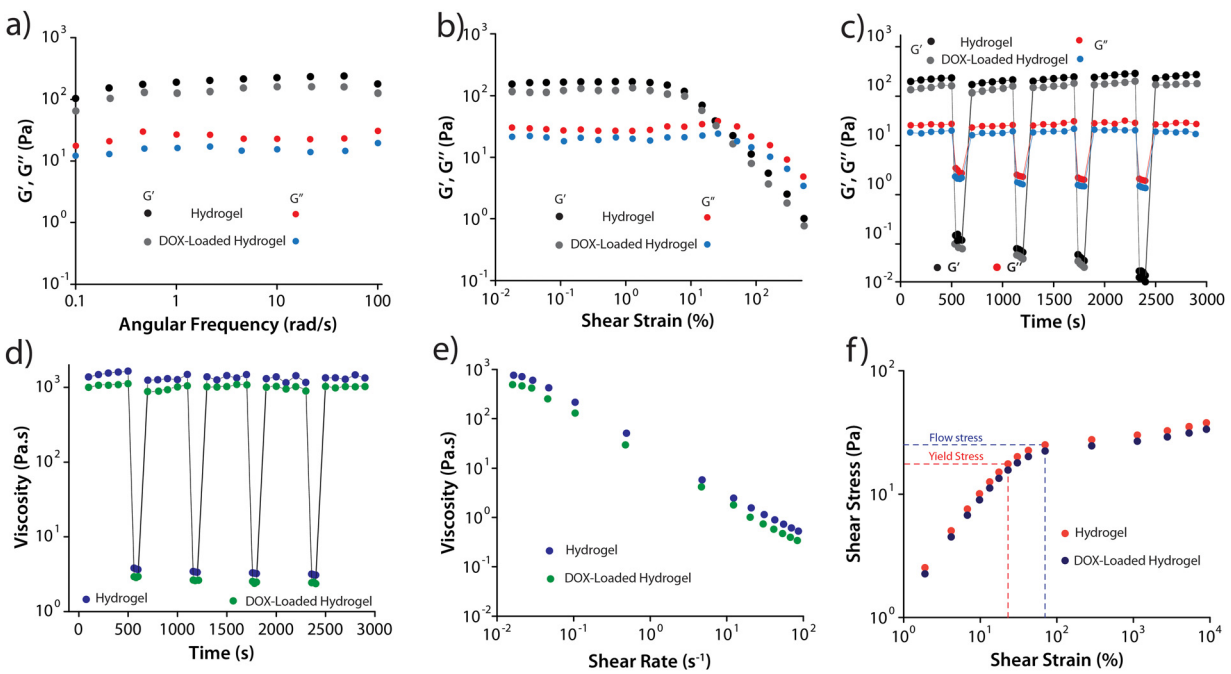

Fig. 2 Rheological analyses of PyKC-hydrogel (1 wt%) with and without DOX (2.5 mM). (a) Frequency sweep and (b) amplitude sweep. (c) Time-dependent step-strain profile showing injectability. (d) Step-shear measurements with alternating high and low shear rates. (e) Steady shear rheology depicting viscosity as a function of shear rate. (f) Flow stress curve depicting the transition from elastic to plastic behavior within the hydrogels.

It was observed that upon applying strain (100%), the gels transformed to sol and reverted back to their original gel state upon strain removal (0.1%). The injectability property (Fig. 2d) was further verified by monitoring the hydrogels' viscosity while alternating between high (100 S^{-1}) and low shear rates (0.01 S^{-1}). In both cases, the viscosity significantly decreased (by three orders of magnitude) under high shear rates and rapidly recovered to the initial viscosity with lower shear strain. The decrease in viscosity with increasing shear rate (Fig. 2e) confirmed the hydrogels' shear-thinning behavior. Fig. 2f illustrates the flow-stress curve, depicting the transition from elastic to plastic behavior within the hydrogels, marked by distinct yield points at 23.1 Pa (PyKC-hydrogel) and 19.8 Pa (DOX-hydrogel). Subsequently, the flow stress increased to 70.5 Pa and 68.2 Pa, respectively, indicating plastic deformation. It is important to note that apart from a slight loss of strength, the presence of DOX in the hydrogel did not affect its rheological properties, especially the injectability.

Next, we wanted to determine whether the presence of DOX imparts any change in the insolubility of the PyKC-hydrogel. Following our previously published protocol, the % dissolution of the DOX-loaded hydrogel in buffers of different pH values was analyzed after incubating the hydrogel samples in the buffers for 7 days. Fig. S2 (ESI†) shows that only approximately 5% dissolution was observed. This minute dissolution was observed within the first hour of incubation, and thus may be attributed to the solubilization of the loosely bound PyKC molecules at the surface of the hydrogel samples.[29] It is noteworthy that the release of DOX from the hydrogel samples, however, was found to be negligible.

To realize targeted therapy, it is important for the hydrogel to engage in GSH-responsive dissolution and subsequent drug release. The GSH concentration in the cancerous cells was found to be approximately 10 times higher than that of normal cells.[38,39] For further evaluation, an *in vitro* release study was performed against varying concentrations (0.1–1000 μM) of GSH (in HBS). Fig. S3 (ESI†) shows the cumulative release profile measured for seven days. It is clear that the dissolution of the hydrogel matrix and, consequently, the release of DOX is highly dependent on the GSH concentration in the bulk incubation medium. A slow and sustained release of DOX was observed when the GSH concentration was in the range of 1–0.1 mM. Even after seven days of incubation, the hydrogels did not completely dissolve, and approximately 32 and 54% DOX were found to be trapped in the hydrogel matrix for 1 and 0.1 mM GSH, respectively.

Enhanced cytotoxic effect of PyKC-hydrogel-incorporated DOX

The non-toxic nature of the PyKC-hydrogel was examined in detail in our previous study.[31] To assess the ability of the PyKC-hydrogel, DOX (5 μM), and DOX (5 μM)-hydrogel to block the proliferation of MDA-MB 231 (human triple-negative breast cancer (TNBC) cell line) and 4T1 (BALB/c mouse breast cancer cell line derived from the mammary gland) cells, MTT assays were performed.[40,41] Their anti-proliferative efficacies in terms of IC_{50} are presented in Fig. 3. The PyKC-hydrogel showed very little cytotoxicity even after 72 h of treatment. Compared to DOX treatment, the DOX (5 μM)-hydrogel treatment exerted significantly higher cytotoxicity and reached the IC_{50} value within 12 h of treatment in both cell lines as compared to DOX (5 μM). The hydrogel releases DOX upon interacting with GSH, leading to a significant depletion of GSH levels in the cytoplasm and nucleus. This depletion disrupts the redox balance and epigenetic regulation, impacting key cell cycle regulators. The resultant oxidative stress elevates reactive oxygen species (ROS) levels, which induces G2/M phase arrest and effectively halts cancer cell proliferation. This mechanism underscores the potent anti-proliferative effects of our DOX-hydrogel system.

Furthermore, to determine the biocompatibility of the PyKC-hydrogel, an MTT assay was conducted on the PyKC-hydrogel-, DOX- (5 μM), and the DOX (5 μM)-hydrogel-treated NKE (normal kidney epithelial) cell line over a 72-hour period. Remarkably, the PyKC-hydrogel and DOX (5 μM)-hydrogel exhibited minimal cytotoxicity even after prolonged exposure, in sharp contrast to the notably higher cytotoxicity of DOX treatment alone, which reached its IC_{50} value within the same time frame (Fig. S4a, ESI†). Based on these results, a 24-h treatment period was selected for further studies of TNBC cell line MDA-MB-231 and 4T1 cancer cells. To re-establish our findings obtained from the MTT assay, phase contrast microscopic imaging of the PyKC-hydrogel-, DOX- (5 μM), and DOX (5 μM)-hydrogel-treated MBA-MB 231, 4T1, and NKE cell lines was performed (Fig. 3b, 3d and Fig. S4b (ESI†), respectively) and SEM analyses of the PyKC-hydrogel-, DOX- (5 μM), and DOX (5 μM)-hydrogel-treated MBA-MB 231 cells were also performed (Fig. 3e).[42]

Our observations revealed that, as compared to the control setup, the treated setup showed a concentration-dependent increase in the level of morphological change to induce death in MDA-MB 231 and 4T1 cells. Our observations in the case of the PyKC-hydrogel-, DOX- (5 μM), and the DOX (5 μM)-hydrogel-treated NKE cell line revealed that treatment with the PyKC-hydrogel and DOX (5 μM)-hydrogel resulted in minimal morphological changes to NKE cells compared to DOX (5 μM) treatment alone (Fig. S4b, ESI†). The results from the SEM analysis of the PyKC-hydrogel-, DOX- (5 μM), and the DOX (5 μM)-hydrogel-treated MDA-MB 231 cell line showed increased apoptotic bodies in the DOX (5 μM)-hydrogel-treated setup in comparison to DOX (5 μM) treatment alone.

The findings from this study highlight the superior cytotoxic effectiveness of combining the PyKC-hydrogel with DOX against TNBC cell line MDA-MB-231 and 4T1 cells. This combination not only achieves significant cytotoxicity at a lower concentration compared to DOX alone, but also underscores the potential of the PyKC-hydrogel as a promising carrier in cancer therapy. Moreover, the non-toxic nature of the PyKC-hydrogel and its combination with DOX suggests reduced cytotoxicity against NKE cells. The diminished release of DOX in DOX (5 μM)-hydrogel-treated NKE cells may be attributed to the lower cytoplasmic GSH concentration in normal cells compared to cancer cells, thereby enhancing the non-toxic efficacy of this combination against NKE cells. These results emphasize the

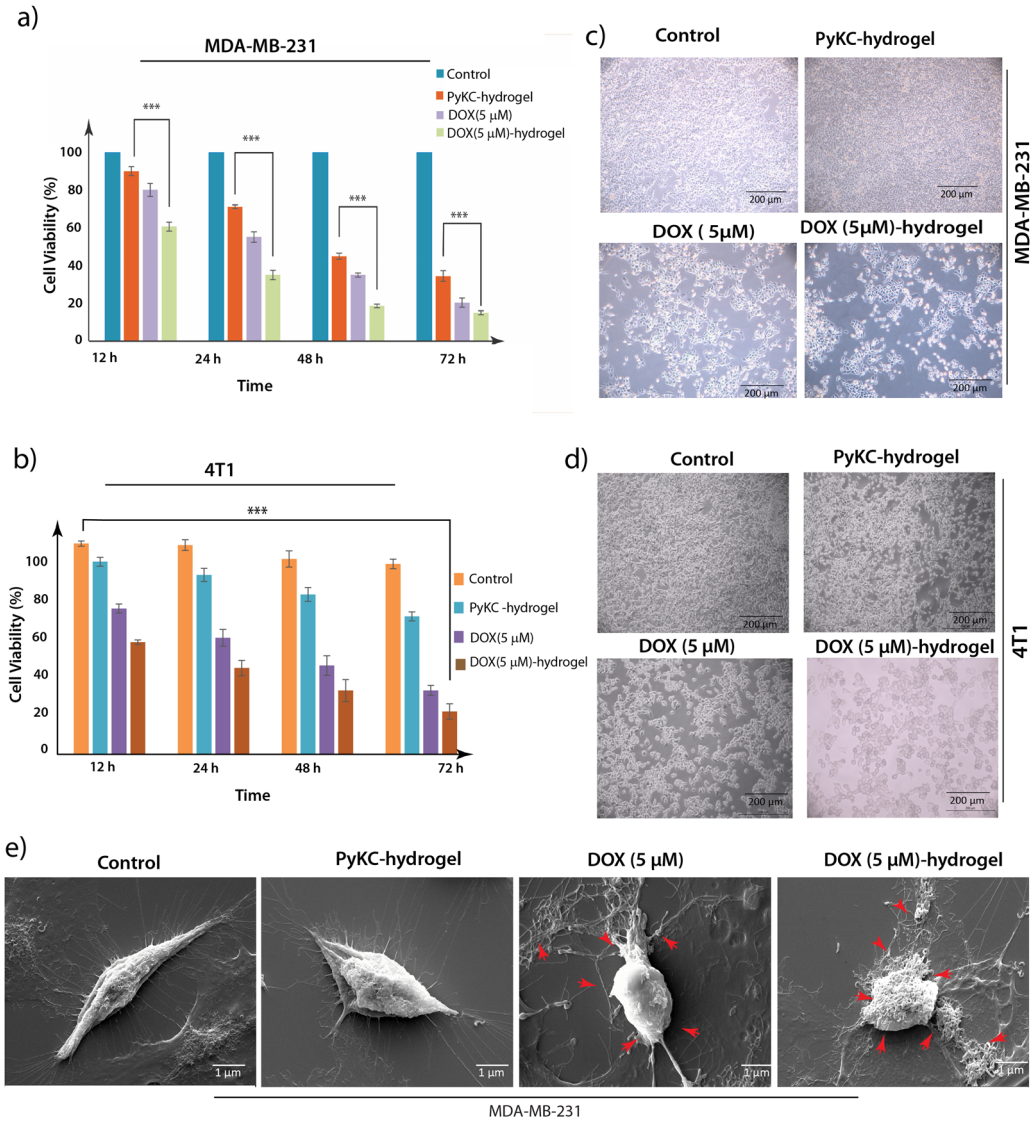

Fig. 3 Cytotoxicity. Cytotoxic activity of the PyKC-hydrogel-, DOX- (5 μM), and DOX (5 μM)-hydrogel-treated (a) MDA-MB-231 cells and (b) 4T1 cells using the MTT assay. Photomicrographs showing the dose-dependent anti-proliferative effect of the PyKC-hydrogel, DOX (5 μM), and DOX (5 μM)-hydrogel on (c) MDA-MB-231 cells and (d) 4T1 cells. All the data are expressed as the mean ± SEM of a minimum of three independent experiments (*$p < 0.05$, **$p < 0.01$, ***$p < 0.001$). (e) SEM images of the PyKC-hydrogel-, DOX- (5 μM), and DOX (5 μM)-hydrogel-treated MDA-MB-231 cells.

potential for safer and more effective cancer treatments with minimization of the dose-related toxicity commonly associated with conventional chemotherapy agents.

Additionally, we conducted a study using MDA-MB-231 cells pre-treated with varying concentrations of GSH (250 μM, 500 μM, and 1000 μM). The cells were incubated with the DOX-loaded hydrogel for 6 hours, washed with PBS, and then analyzed using fluorescence microscopy to assess DOX uptake. Our results (Fig. S5, ESI†) show a clear increase in DOX uptake, indicated by increased red fluorescence within the cells, which was correlated with higher GSH concentrations. These results strongly support the conclusion that DOX release from the hydrogel is triggered by elevated intracellular GSH, which results in enhanced cytotoxicity in cancer cells.

DOX-loaded PyKC-hydrogel induces G2/M phase arrest and enhances apoptosis in cancer cells

Following the MTT assay, which provided initial insights into the cytotoxic efficacy of DOX-loaded PyKC-hydrogel against MDA-MB 231 and 4T1 cancer cells, further investigation into the underlying mechanisms of cell growth inhibition was warranted. The MTT assay, by revealing a significant reduction in cell viability, laid the groundwork for deeper exploration into how this treatment affects cell cycle dynamics and induces cell death. Consequently, to elucidate these mechanisms, we conducted a flow cytometric analysis focusing on cell cycle distribution and apoptotic cell death, aiming to understand the specific phases of cell cycle arrest and the predominant mode of cell death induced by the treatment.

To ascertain the nature of cell death—whether it was primarily apoptotic or involved other cell death pathways—Annexin V-FITC/PI staining followed by flow cytometric analyses were performed. This method distinguished between live, early apoptotic, late apoptotic, and necrotic cells.[43] The results showed a marked increase in apoptotic cells among the DOX (5 μM)-hydrogel-treated groups (54.23% in MDA-MB-231 cells and 40.96% in 4T1 cells) compared to DOX treatment alone (41.58% apoptotic MDA-MB-231 cells and 30.79% apoptotic 4T1 cells) (Fig. 4a–d). Additionally, the results from the Annexin V-FITC assay of the PyKC-hydrogel-, DOX- (5 μM), and DOX (5 μM)-hydrogel-treated NKE cells demonstrated a substantial increase in the apoptotic cell population (41.11%) following DOX (5 μM) treatment, whereas the PyKC-hydrogel and DOX (5 μM) + hydrogel groups exhibited significantly lower levels of apoptotic cell death, at 14.95% and 15.58%, respectively (Fig. S4c, ESI†). These findings strongly support the non-toxic nature of the PyKC-hydrogel and indicate that the combination of PyKC-hydrogel with DOX leads to reduced cytotoxicity against NKE cells compared to DOX treatment alone.

Flow cytometric analysis of cell cycle distribution revealed a notable increase in the G2/M phase population in MDA-MB-231 (51.60%) and 4T1 (43.18%) cells treated with the DOX (5 μM)-hydrogel, as compared to cells treated with DOX alone (23.67% in MDA-MB-231 and 31.28% in 4T1 cells). This was accompanied by a corresponding decrease in the G1 phase cell population, indicating a significant G2/M arrest. Such arrest in the G2/M phase is critical because it indicates a halt in cell division,

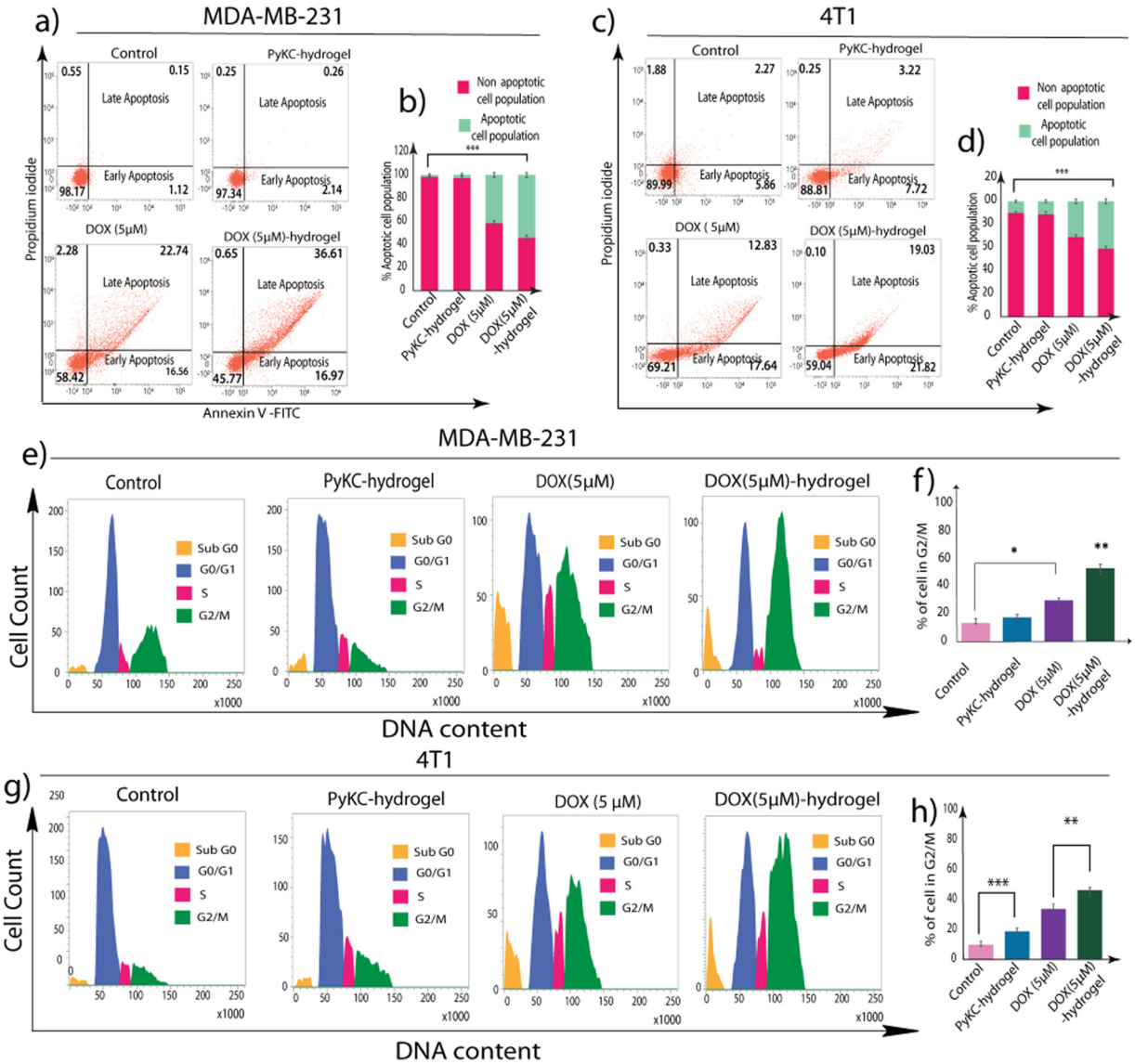

Fig. 4 Quantification of apoptosis induction. (a–d) Flow cytometric analysis of the PyKC-hydrogel-, DOX- (5 μM), and DOX (5 μM)-hydrogel-treated MDA-MB-231 cells and 4T1 cells that were stained with Annexin V-FITC/PI. (e–h) Cell cycle profiling assay of the PyKC-hydrogel-, DOX- (5 μM), and DOX (5 μM)-hydrogel-treated MDA-MB-231 cells and 4T1 cells by propidium iodide (PI) staining using a BD FACSVerse flow cytometer. All the data are expressed as the mean ± SEM of a minimum of three independent experiments (*$p < 0.05$, **$p < 0.01$, ***$p < 0.001$).

which is a precursor to apoptosis in many forms of cancer therapy (Fig. 4e–h).

The combined data from these experiments indicate that the DOX (5 μM)-hydrogel treatment inhibits cell proliferation, as evidenced by the MTT assay, and it also exerts its anti-proliferative effects through specific mechanisms. It induces a significant arrest in the G2/M phase of the cell cycle and promotes apoptotic cell death in MDA-MB-231 and 4T1 cancer cells.

Enhanced ROS accumulation and DNA fragmentation by DOX-loaded PyKC-hydrogel

Following the identification of cell cycle arrest and apoptotic cell death induced by the DOX (5 μM)-hydrogel treatment in MDA-MB 231 and 4T1 cells, it became imperative to delve into the underlying mechanisms contributing to these observations. ROS are known to be double-edged swords within biological systems. While they are vital for several signaling processes, excessive ROS levels can lead to oxidative stress that damages cellular components and results in apoptosis.[43] Therefore, investigating ROS accumulation after observing G2/M arrest and increased apoptotic cell death is the logical next step.

To this end, the H2DCFDA fluorescence assay was employed to detect ROS generation within the cells. This method hinges on the principle that the non-fluorescent H2DCFDA dye, upon entering the cell, is oxidized by ROS to form a green fluorescent compound, thereby serving as an indicator of ROS levels.[44] Fluorescence microscopy and flow cytometric analyses were utilized to visualize and quantify ROS accumulation. The fluorescence microscopic

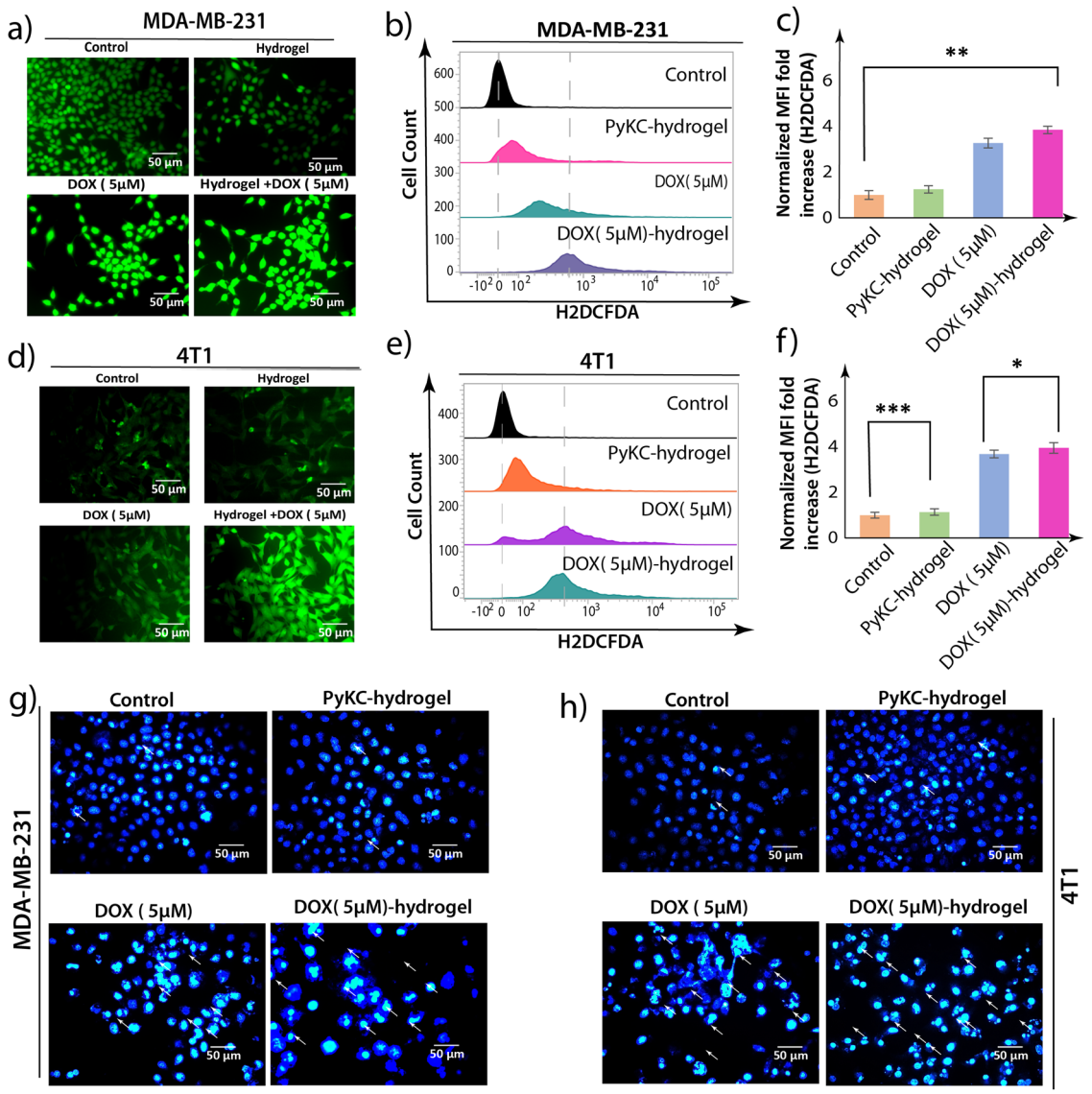

Fig. 5 Effect of the PyKC-hydrogel on ROS production. Microscopic and flow cytometric analyses to estimate the intercellular reactive oxygen species (ROS) production within (a)–(c) MDA-MB-231 cells and (d)–(e) 4T1 cells using the DCFDA method after treatment with PyKC-hydrogel, DOX (5 μM), and DOX (5 μM)-hydrogel. Apoptotic nuclear morphology study by DAPI staining of (g) MDA-MB-231 cells and (h) 4T1 cells after treatment with PyKC-hydrogel, DOX (5 μM), and DOX (5 μM)-hydrogel. All the data are expressed as the mean ± SEM of a minimum of three independent experiments (*$p < 0.05$, **$p < 0.01$, ***$p < 0.001$).

images revealed a significant increase in green fluorescent intensity in MDA-MB 231 and 4T1 cells treated with DOX (5 μM)-hydrogel, indicative of heightened ROS levels compared to the control, and PyKC-hydrogel- and DOX-treated cells. This was corroborated by the flow cytometric data, which showed an elevated mean fluorescent intensity (MFI) in cells treated with the DOX (5 μM)-hydrogel, further confirming the increased ROS accumulation (Fig. 5a–f).

Staining with 4′,6-diamidino-2-phenylindole (DAPI)[45] also showed an increased level of polynuclear fragmentation and nuclear shrinking in DOX (5 μM)-hydrogel-treated MDA-MB-231 and 4T1 cells in comparison to DOX (5 μM)-treated MDA-MB 231 and 4T1 cells. In comparison, very little polynuclear fragmentation or nuclear shrinking was observed in control and hydrogel-treated MDAMB-231 and 4T1 cells (Fig. 5g and h).

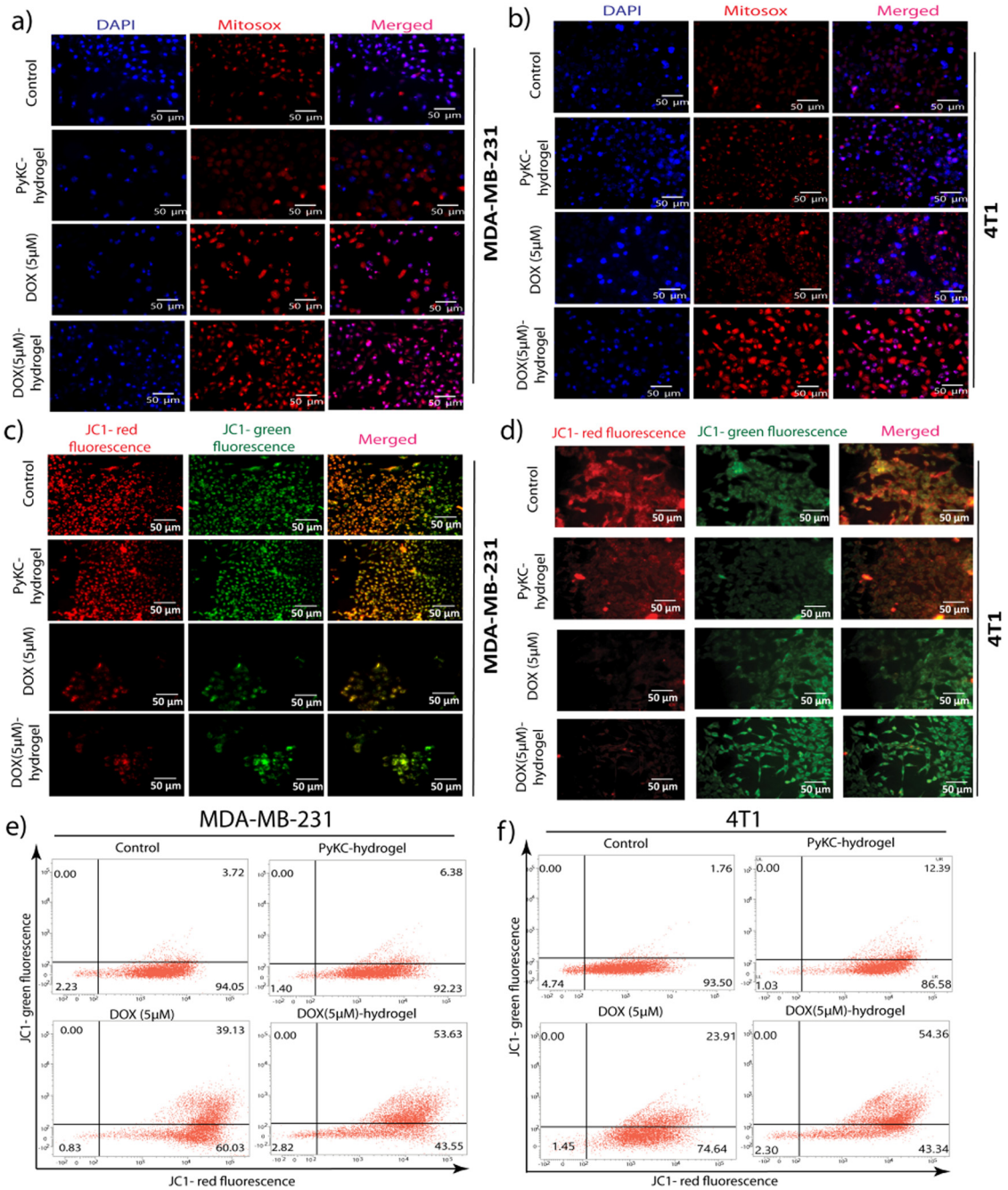

Fig. 6 Mitochondrial membrane potential disruption. (a) and (b) Fluorescent microscopic images of mitochondrial ROS accumulation in MitoSOX-stained (a) MDA-MB-231 cells and (b) 4T1 cells due to PyKC-hydrogel, DOX (5 μM), and DOX (5 μM)-hydrogel treatment. Fluorescence microscopic and flow cytometric analysis using JC-1 staining to estimate the changes in mitochondrial membrane permeability in (c) and (e) MDA-MB-231 cells and (d) and (f) 4T1 cells due to PyKC-hydrogel, DOX (5 μM), and DOX (5 μM)-hydrogel treatment.

These experiments collectively suggest that the enhanced apoptosis of MDA-MB 231 and 4T1 cells triggered by the DOX-loaded hydrogel is mediated through the accumulation of intracellular ROS. This ROS generation is a key upstream event that leads to G2/M phase arrest and also underscores the importance of the DOX (5 μM)-hydrogel not only in directly inducing apoptosis, but also in influencing the cellular oxidative environment to promote cell death, and thus offering a multi-faceted approach to cancer therapy.

Mitochondrial ROS generation and mitochondrial membrane potential disruption by DOX (5 μM)-hydrogel treatment

Following the comprehensive examination of cell cycle arrest, apoptosis, and ROS accumulation induced by DOX-loaded PyKC-hydrogel, it became imperative to delve into its effects on mitochondrial redox homeostasis. GSH is pivotal in cellular redox equilibrium, serving as a primary antioxidant by scavenging reactive oxygen species (ROS). Hence, any disruption in GSH levels can exert profound repercussions on cellular physiology, notably on mitochondrial function.[46] Consequently, as PyKC interacts with GSH, leading to the downregulation of free GSH levels, it was imperative to explore the ramifications of the DOX-loaded PyKC-hydrogel on mitochondrial ROS accumulation.

Subsequently, MitoSOX staining emerged as a vital tool for scrutinizing mitochondrial ROS generation because it is renowned for its ability to distinguish between healthy and ROS-burdened mitochondria.[47] An elevation in MitoSOX red fluorescence signifies mitochondrial ROS accumulation, and

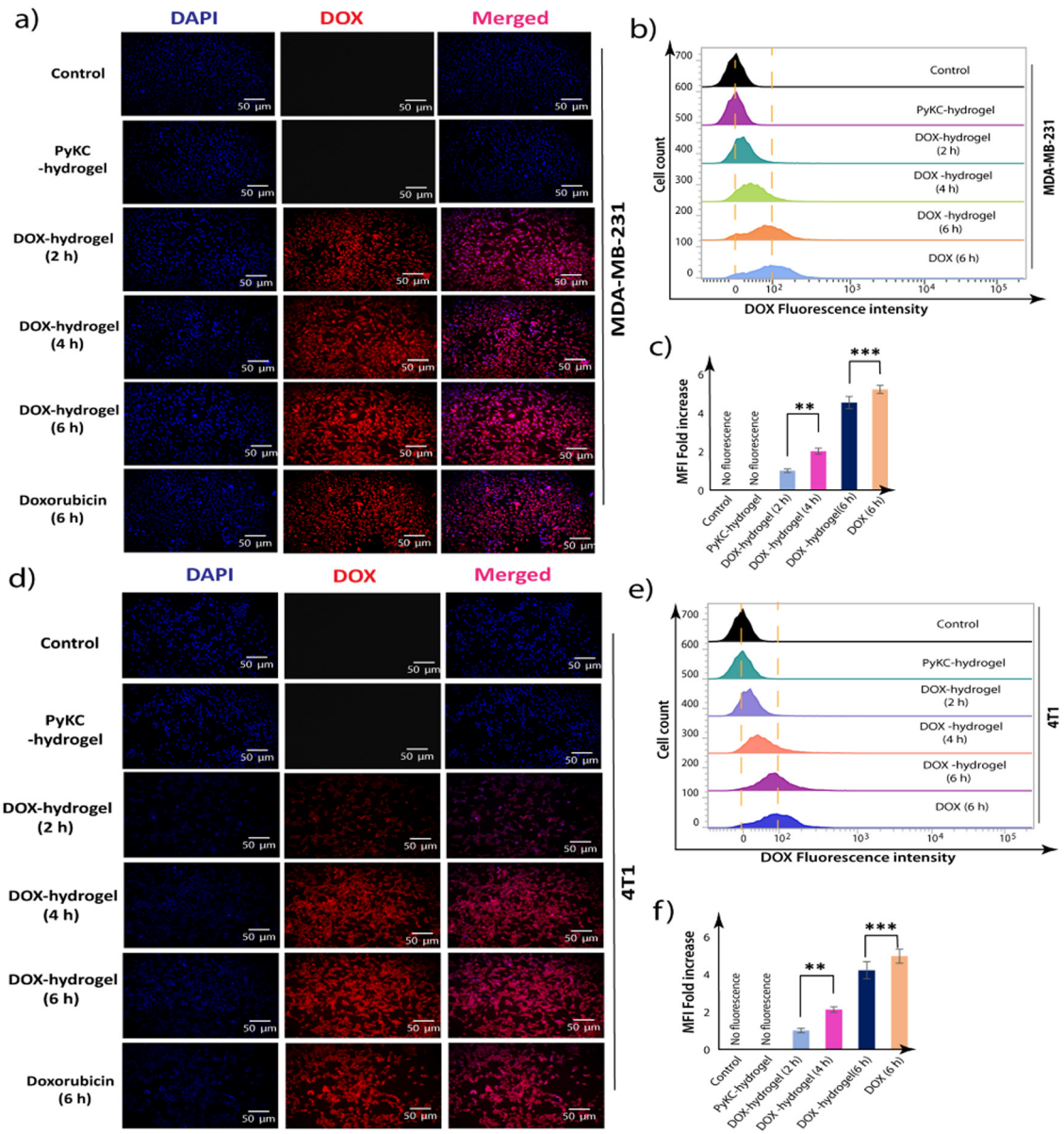

Fig. 7 Internalization of DOX by cancer cells. Fluorescence microscopic (a) and (d) and flow cytometric analyses of the cellular uptake of DOX in (b) and (c) MDA-MB-231 and (e), (f) 4T1 cells upon incubation for different durations. All the data are expressed as the mean ± SEM of a minimum of three independent experiments (*$p < 0.05$, **$p < 0.01$, ***$p < 0.001$).

serves as a mark of perturbed redox balance within the cell. The experimental findings unveiled a conspicuous surge in red fluorescence intensity in MDA-MB 231 and 4T1 cells treated with DOX (5 μM)-hydrogel, indicative of significant mitochondrial ROS accumulation (Fig. 6a and b). This effect manifested more prominently compared to cells treated solely with DOX (5 μM), untreated control cells, and those treated exclusively with the PyKC-hydrogel. Such observations underscore the potent impact of the DOX-loaded PyKC-hydrogel on cellular physiology, particularly on mitochondrial function and redox equilibrium.

Further investigation was needed to determine the effects on the mitochondrial membrane potential (MMP). The disruption of the MMP is a hallmark of the intrinsic pathway of apoptosis, and it acts as a pivotal event that orchestrates cell death mechanisms.[48] Given that excessive ROS production can impair mitochondrial function and lead to the loss of MMP, examining the state of the MMP after the establishment of ROS accumulation bridges our understanding of how DOX (5 μM)-hydrogel treatment triggers apoptosis at a cellular level. JC-1 staining, a widely used method for assessing MMP, differentiates healthy mitochondria (red fluorescence) from those with compromised membrane potential (green fluorescence).[42] A shift from red to green fluorescence indicates a decrease in MMP, which signifies early apoptotic changes before nuclear condensation and fragmentation occur.[42]

The findings revealed through JC-1 staining demonstrated a noticeable increase in green fluorescence intensity, corresponding to a decrease in the red/green fluorescence intensity ratio in MDA-MB 231 and 4T1 cells treated with the DOX (5 μM)-hydrogel. This shift was more pronounced compared to cells treated with DOX (5 μM) alone, untreated control, or PyKC-hydrogel-treated cells (Fig. 6c and d). Flow cytometric analyses further confirmed these observations, indicating a significant disruption in MMP among cells subjected to the DOX-hydrogel combination (Fig. 6e and f).

The investigation into MMP disruption post-treatment with DOX (5 μM)-hydrogel provides critical insight into the mechanism of apoptosis induction by this therapeutic combination. Following evidence of cell cycle arrest, enhanced apoptosis, and ROS generation, the observed decrease in MMP underscores the activation of the mitochondrial pathway of apoptosis. This sequence of cellular events illustrates a comprehensive apoptotic cascade initiated by DOX (5 μM)-hydrogel treatment, from external stressors leading to ROS accumulation to internal mitochondrial distress manifesting as MMP disruption, culminating in cell death.

Enhanced intracellular uptake of DOX-loaded PyKC-hydrogel

One of the significant challenges in DOX therapy is achieving an optimal intracellular concentration; too little results in a lack of efficacy against cancer cells, while too much can lead to toxicity in healthy cells.[49] Therefore, examining the uptake of DOX, especially when encapsulated or combined with delivery systems, is crucial for evaluating the potential for enhanced therapeutic outcomes. The rationale behind

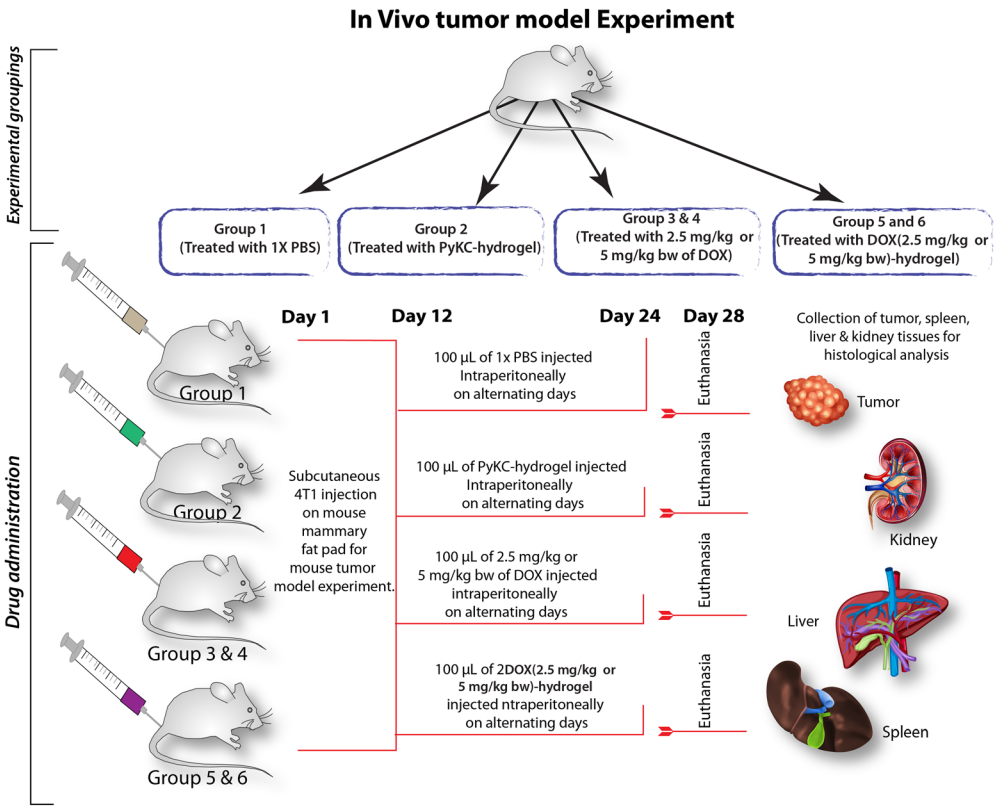

Fig. 8 Schematic representation of *in vivo* tumor model experiments.

studying DOX uptake in combination with the PyKC-hydrogel is twofold. First, to ascertain if the hydrogel can improve the cellular internalization of DOX, thereby potentially increasing its anticancer activity by ensuring that a greater amount of the drug will reach its intracellular targets. Second, to determine if the release and uptake of DOX can be controlled or modified to be more efficient over time, which could lead to a reduction in the required dosage and associated side effects.

Flow cytometric analyses were employed to quantify the intracellular localization and accumulation of DOX in MDA-MB-231 and 4T1 cells treated with PyKC-hydrogel, DOX-hydrogel, and free DOX over 2, 4, and 6 hours. The results demonstrated a time-dependent increase in the intracellular concentration of DOX. Notably, after 6 hours of incubation, cells treated with DOX- showed a significant enhancement in DOX uptake efficiency in MDA-MB-231 and 4T1 cell hydrogel lines (Fig. 7). This observation

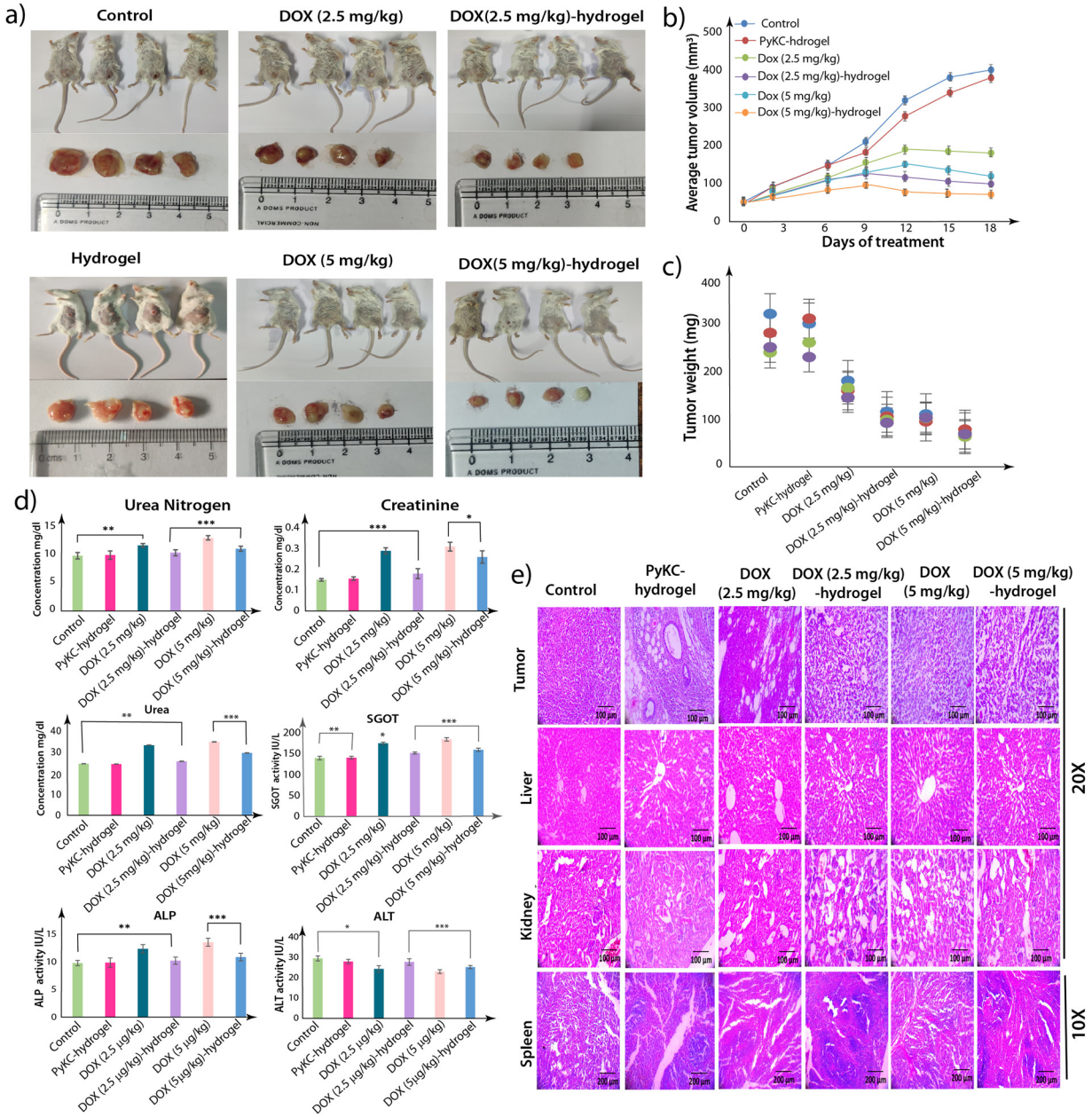

Fig. 9 *In vivo* DOX release. (a) Images of euthanized mice with the tumors and the isolated dissected tumors. (b) The graph represents the volume of the dissected tumors at various time points during treatment. (c) The weight of the tumors is represented here. (d) Evaluation of the toxicity in the blood serum after treatment. (the bar graphs indicate the various parameters evaluated for the toxicity of the compound). The normal mice were treated with the PyKC-hydrogel, DOX (2.5 mg kg^{-1}), DOX (2.5 mg kg^{-1})-hydrogel, DOX (5 mg kg^{-1}), or DOX (5 mg kg^{-1})-hydrogel for 14 days. (e) Phase contrast microscopic images of tissues from different organs of the treated mice. The tissues were stained with H&E. The images were captured at 20× and 10× magnification with a Leica phase contrast microscope. The data are representative of three independent testings, and the bar graph displays the mean ± SEM (*$p < 0.05$, **$p < 0.01$, ***$p < 0.001$).

underscores the efficacy of PyKC-hydrogel as a delivery vehicle, which enhanced DOX internalization into cancer cells, an action that is critical for optimizing the anticancer activity of DOX. Enhanced uptake facilitated by PyKC-hydrogel could lead to more effective cancer cell targeting and destruction, and presents a promising avenue for improving the therapeutic outcomes in breast cancer treatment.

Superior tumor size reduction by DOX-loaded PyKC-hydrogel

After obtaining enhanced anticancer activity in *in vitro* studies, *in vivo* studies using female BALB/c mice were performed to determine the efficacy, safety, and overall therapeutic potential of the DOX-loaded PyKC-hydrogel within a more complex biological system that closely mimics human physiology and pathology.[50,51] The *in vivo* study utilizing a mouse breast cancer tumor model provides crucial insights into the therapeutic efficacy and safety profile of the DOX-loaded PyKC-hydrogel. By employing female BALB/c mice with palpable tumors, this study aimed to evaluate the effects of different treatment regimens on tumor size, physical abnormalities, and histological changes in various tissues, as well as toxicity markers.

In this investigation, we established a breast cancer model utilizing female BALB/c mice. The flowchart of the experiment is provided in Fig. 8. Regular measurements of tumor size were conducted every third day following palpable tumor development. After the seventh treatment cycle, a remarkable reduction in tumor size was observed in the groups receiving DOX (2.5 mg kg^{-1})-hydrogel and DOX (5 mg kg^{-1})-hydrogel, in stark contrast to those treated solely with DOX at equivalent doses (Fig. 9a–c). Conversely, the tumor size in the control and the PyKC-hydrogel-treated groups remained relatively stable, with minimal changes in volume. Notably, mice treated with PyKC-hydrogel, DOX (2.5 mg kg^{-1})-hydrogel, and DOX (5 mg kg^{-1})-hydrogel did not manifest any discernible physical abnormalities, such as hair loss, weight gain, or impairment in vision or orientation, unlike the DOX-treated groups, which exhibited varying degrees of physical abnormalities, including weight loss and hair thinning.

Following treatment completion, the mice were euthanized, and various tissue samples, including tumors, kidneys, liver, and spleen, were harvested. These samples underwent processing, paraffin embedding, and subsequent hematoxylin and eosin (H&E) staining. Histological examination revealed a notable decrease in tumor cell compactness post-treatment, with some cells exhibiting signs of loss (Fig. 9d). Similar restorative changes were observed in kidney, spleen, and liver tissues following treatment.

Furthermore, serum samples were promptly collected upon euthanasia, and concentrations of urea, urea nitrogen,

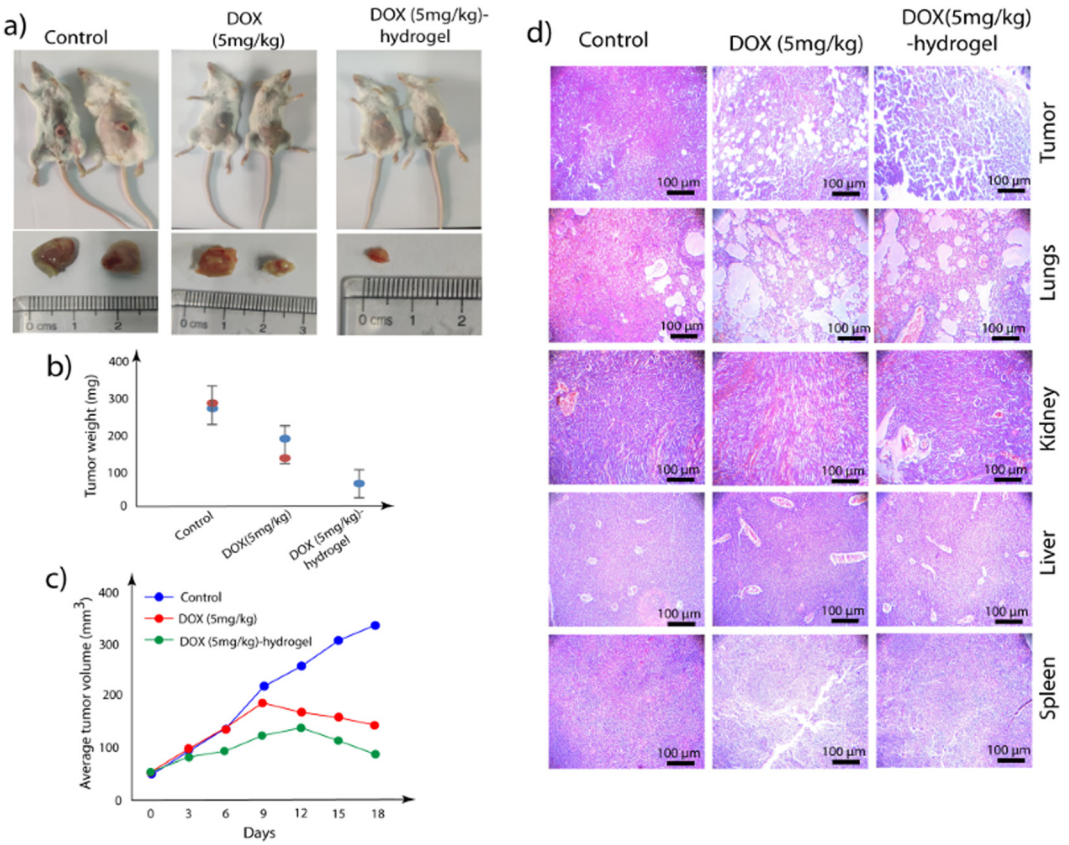

Fig. 10 Effect of a single injection. (a) Images of euthanized mice with tumors and isolated dissected tumors. (b) The weight of the tumors from different groups of mice. (c) The graph represents the volume of the dissected tumors at various time points during treatment. (d) Phase contrast microscopic images of tissues from different organs of the treated mice. The tissues were stained with H&E. A Leica phase contrast microscope was used to capture the images at 20× and 10× magnification.

creatinine, aspartate aminotransferase (AST), alanine aminotransferase (ALT), and alkaline phosphatase (ALP) were meticulously measured. No significant changes in body weight were observed among the mice, and most toxicity parameters remained within the normal range, except for certain alterations noted in the DOX 2.5 mg kg^{-1}- and DOX 5 mg kg^{-1}-treated groups (Fig. 9e). Collectively, these findings underscore the efficacy and safety profile of the hydrogel combined with a DOX treatment regimen in a mouse breast cancer model, warranting further exploration of this promising therapeutic strategy in clinical contexts.

Effect of a single injection of DOX-loaded hydrogel

Encouraged by the *in vivo* studies, we then evaluated the effect of a single injection of the DOX-loaded PyKC-hydrogel on the tumor. Two groups of mice were treated with a single injection of either DOX (5 mg kg^{-1}) or DOX (5 mg kg^{-1})-hydrogel, while the third group was left untreated as a control. Regular measurements of tumor size were conducted every third day following palpable tumor development. After 18 days, the mice were euthanized, and various tissue samples, including tumors, kidneys, liver, and spleen, were harvested.

A remarkable reduction in the tumor size (approximately 75%) was observed in the group receiving DOX (5 mg kg^{-1})-hydrogel treatment compared to the control and DOX-treated groups (Fig. 10a–c). Notably, mice treated with the DOX (5 mg kg^{-1})-hydrogel did not show any observable physical abnormalities. The DOX-treated groups exhibited varying degrees of physical abnormalities, including weight loss and hair thinning. The histological examination of the collected tumors and other tissues revealed a notable decrease in tumor cell compactness post-treatment, with some cells exhibiting signs of loss (Fig. 10d). Similar curative changes were observed in other tissues.

The hydrogel-based delivery vehicle significantly reduced the tumor size after a single dose, and therefore, it was important to analyze the status of the injected gels near the tumors after 18 days. For evaluation, the collected tumors were washed in PBS buffer (1 mL), and the solutions were analyzed using high-performance liquid chromatography (HPLC) and fluorescence spectroscopy. Interestingly, while no DOX was observed for DOX (5 mg kg^{-1})-treated samples, clear HPLC peaks of DOX, PyKC monomer, and PyKC dimers were observed in the DOX (5 mg kg^{-1})-hydrogel-treated sample (Fig. S6, ESI†). The fluorescence analyses also support the presence of DOX and PyKC in the DOX (5 mg kg^{-1})-hydrogel-treated sample, while nothing was observed in the DOX (5 mg kg^{-1})-treated sample (Fig. S7, ESI†).

Conclusion

The development of a GSH-responsive localized drug delivery system using an injectable ultra-short peptide-based hydrogel presents a significant advancement in cancer treatment. By addressing the limitations of conventional chemotherapy, such as systemic toxicity and limited drug efficacy, this innovative approach offers targeted and sustained release of drugs directly to the tumor site. Because of the unique properties of the PyKC-hydrogel, including its injectability, insolubility, and GSH responsiveness, it is a promising candidate for localized drug delivery. Rheological studies confirmed that the presence of DOX did not compromise the mechanical properties of the hydrogel, ensuring its effectiveness as a drug carrier. *In vitro* studies demonstrated that compared to free DOX, there was an enhanced cytotoxic effect of the DOX-loaded PyKC-hydrogel that significantly inhibited cancer cell proliferation.

Mechanistic insights revealed that the DOX-loaded hydrogel induced G2/M phase cell cycle arrest that promoted apoptotic cell death and triggered ROS accumulation, highlighting its multi-faceted approach to cancer therapy. Furthermore, the hydrogel facilitated enhanced intracellular uptake of DOX, offering the potential for improved therapeutic outcomes with reduced dosages and side effects. Notably, the *in vivo* studies with a single injection of DOX-loaded PyKC-hydrogel resulted in approximately 75% reduction of the tumor within 18 days and no noticeable impact on other organs. These observations signify the effectiveness of the hydrogel as a sustained delivery vehicle. Overall, this study underscores the efficacy and potential of the PyKC-hydrogel as a localized drug delivery system for breast cancer treatment, paving the way for future clinical applications and personalized medicine approaches in cancer therapy.

Experimental

The detailed experimental procedure is provided in the ESI.†

Ethical statement

The animal testing was performed with approval from the Institutional Animal Ethics Committee (IAEC) of Bose Institute, Kolkata, following standard guidelines.

Author contributions

D. D. conceptualized the idea. The synthesis of PyK, rheology, *in vitro* release, and other characterization studies were performed by T. D. and R. K. The biological studies were planned, executed, and analyzed by S. H., and K. J. A. K. M. provided resources. All authors contributed in preparing the manuscript.

Data availability

The data that support the findings of this study are available in the ESI† of this article.

Conflicts of interest

The authors declare no conflicts of interest. The authors declare that the Indian Patent Number 417150, awarded on 09/01/2023, is related to the hydrogel used for this study.

Acknowledgements

R. K. acknowledges the Ministry of Education (MoE), Government of India, for providing the Prime Minister's Research Fellowship (PMRF). SH thanks UGC for providing the JRF & SRF fellowship (19/06/2016(i) EU-V). D. D. acknowledges financial support from SERB, India (CRG 2020/002030), BRNS, India (58/14/05/2022), and the FIST program for the Department of Chemistry, IIT Guwahati. The authors also thank CLART and WBLDC for supporting the animal experiments, and Dr Ananya Dutta, former SRF, Division of Molecular Medicine, for the conceptualization of this study with an animal model.

References

1 V. Conca, P. Ciracì, C. Boccaccio, A. Minelli, C. Antoniotti and C. Cremolini, *Cancer Treat. Rev.*, 2024, **126**, 102735.
2 E. Bidram, Y. Esmaeili, H. Ranji-Burachaloo, N. Al-Zaubai, A. Zarrabi, A. Stewart and D. E. Dunstan, *J. Drug Delivery. Sci. Technol.*, 2019, **54**, 101350.
3 E. Bidram, Y. Esmaeili, H. Ranji-Burachaloo, N. Al-Zaubai, A. Zarrabi, A. Stewart and D. E. Dunstan, *J. Drug Delivery Sci. Technol.*, 2019, **54**, 101350.
4 S. Tohme, R. L. Simmons and A. Tsung, *Cancer Res.*, 2017, **77**, 1548–1552.
5 O. S. Fenton, K. N. Olafson, P. S. Pillai, M. J. Mitchell and R. Langer, *Adv. Mater.*, 2018, **30**, 1705328.
6 P. Kabos and V. F. Borges, in *Early Diagnosis and Treatment of Cancer Series: Breast Cancer*, ed. L. Jacobs and C. A. Finlayson, W.B. Saunders, Saint Louis, 2011, pp. 307–318.
7 M. S. Sabel, in *Essentials of Breast Surgery*, ed. M. S. Sabel, Mosby, Philadelphia, 2009, pp. 307–322.
8 G. K. Alderton, *Nat. Rev. Cancer*, 2014, **14**, 298.
9 D. J. Benjamin, *Med. Hypotheses*, 2014, **82**, 412–420.
10 S. Senapati, A. K. Mahanta, S. Kumar and P. Maiti, *Signal Transduction Target. Ther.*, 2018, **3**, 7.
11 J. Gao, J. M. Karp, R. Langer and N. Joshi, *Chem. Mater.*, 2023, **35**, 359–363.
12 S. Mura, J. Nicolas and P. Couvreur, *Nat. Mater.*, 2013, **12**, 991–1003.
13 Q. Zhou, S. Shao, J. Wang, C. Xu, J. Xiang, Y. Piao, Z. Zhou, Q. Yu, J. Tang, X. Liu, Z. Gan, R. Mo, Z. Gu and Y. Shen, *Nat. Nanotechnol.*, 2019, **14**, 799–809.
14 W. Zhang, M. Wang, W. Tang, R. Wen, S. Zhou, C. Lee, H. Wang, W. Jiang, I. M. Delahunty, Z. Zhen, H. Chen, M. Chapman, Z. Wu, E. W. Howerth, H. Cai, Z. Li and J. Xie, *Adv. Mater.*, 2018, **30**, 1805557.
15 I. de Lázaro and D. J. Mooney, *Nat. Mater.*, 2021, **20**, 1469–1479.
16 A. M. Vargason, A. C. Anselmo and S. Mitragotri, *Nat. Biomed. Eng.*, 2021, **5**, 951–967.
17 M. Hauck, D. Hellmold, C. Kubelt, M. Synowitz, R. Adelung, F. Schütt and J. Held-Feindt, *Adv. Healthcare*, 2022, **5**, 2200013.
18 A. K. Grosskopf, L. Labanieh, D. D. Klysz, G. A. Roth, P. Xu, O. Adebowale, E. C. Gale, C. K. Jons, J. H. Klich, J. Yan, C. L. Maikawa, S. Correa, B. S. Ou, A. I. d'Aquino, J. R. Cochran, O. Chaudhuri, C. L. Mackall and E. A. Appel, *Sci. Adv.*, 2022, **8**, eabn8264.
19 T. Ji and D. S. Kohane, *Nano Today*, 2019, **28**, 100765.
20 M. R. Shah, M. Imran and S. Ullah, in *Nanocarriers for Organ-Specific and Localized Drug Delivery*, ed. M. R. Shah, M. Imran and S. Ullah, Elsevier, 2022, pp. 135–166.
21 G. A. Roth, E. C. Gale, M. Alcántara-Hernández, W. Luo, E. Axpe, R. Verma, Q. Yin, A. C. Yu, H. Lopez Hernandez, C. L. Maikawa, A. A. A. Smith, M. M. Davis, B. Pulendran, J. Idoyaga and E. A. Appel, *ACS Cent. Sci.*, 2020, **6**, 1800–1812.
22 Y. C. Kim, M. D. Shin, S. F. Hackett, H. T. Hsueh, R. Lima e Silva, A. Date, H. Han, B.-J. Kim, A. Xiao, Y. Kim, L. Ogunnaike, N. M. Anders, A. Hemingway, P. He, A. S. Jun, P. J. McDonnell, C. Eberhart, I. Pitha, D. J. Zack, P. A. Campochiaro, J. Hanes and L. M. Ensign, *Nat. Biomed. Eng.*, 2020, **4**, 1053–1062.
23 C. Bastiancich, P. Danhier, V. Préat and F. Danhier, *J. Controlled Release*, 2016, **243**, 29–42.
24 V. G. Muir and J. A. Burdick, *Chem. Rev.*, 2021, **121**, 10908–10949.
25 G. W. Liu, M. J. Pickett, J. L. P. Kuosmanen, K. Ishida, W. A. M. Madani, G. N. White, J. Jenkins, S. Park, V. R. Feig, M. Jimenez, C. Karavasili, N. B. Lal, M. Murphy, A. Lopes, J. Morimoto, N. Fitzgerald, J. H. Cheah, C. K. Soule, N. Fabian, A. Hayward, R. Langer and G. Traverso, *Nat. Mater.*, 2024, **23**, 1292–1299.
26 T. A. Adjuik, S. E. Nokes and M. D. Montross, *J. Appl. Polym. Sci.*, 2023, **140**, e53655.
27 P. Das and D. Das, in *Peptide Bionanomaterials: From Design to Application*, ed. M. A. Elsawy, Springer International Publishing, Cham, 2023, pp. 145–194.
28 S. Das and D. Das, *Front. Chem.*, 2021, **9**, 770102.
29 N. Singha, A. Srivastava, B. Pramanik, S. Ahmed, P. Dowari, S. Chowdhuri, B. K. Das, A. Debnath and D. Das, *Chem. Sci.*, 2019, **10**, 5920–5928.
30 N. Singha, B. K. Das, B. Pramanik, S. Das and D. Das, *Chem. Sci.*, 2019, **10**, 10035–10039.
31 M. M. Islam, A. Chivu, D. B. AbuSamra, A. Saha, S. Chowdhuri, B. Pramanik, C. H. Dohlman, D. Das, P. Argüeso, J. Rajaiya, H. K. Patra and J. Chodosh, *Sci. Rep.*, 2022, **12**, 9108.
32 S. Chowdhuri, M. Ghosh, L. Adler-Abramovich and D. Das, *Pharmaceutics*, 2021, **13**, 1602.
33 D. Das and N. Singha, *India Pat.*, 417150, 2023.
34 S. Chowdhuri, S. Das, R. Kushwaha, T. Das, B. K. Das and D. Das, *Chem. – Eur. J.*, 2023, **29**, e202203820.
35 N. Traverso, R. Ricciarelli, M. Nitti, B. Marengo, A. L. Furfaro, M. A. Pronzato, U. M. Marinari and C. Domenicotti, *Oxid. Med. Cell. Longev.*, 2013, **2013**, 972913.
36 L. Kennedy, J. K. Sandhu, M. E. Harper and M. Cuperlovic-Culf, *Biomolecules*, 2020, **10**, 1429.
37 T. Das, S. Das and D. Das, *Chem. Eng. J.*, 2023, **477**, 147105.
38 H. J. Forman, H. Zhang and A. Rinna, *Mol. Asp. Med.*, 2009, **30**, 1–12.
39 P. Liu, L. Hao, M. Liu and S. Hu, *Front. Bioeng. Biotechnol.*, 2023, **11**, 1161472.

40 J. van Meerloo, G. J. Kaspers and J. Cloos, *Methods Mol. Biol.*, 2011, **731**, 237–245.
41 M. Ghasemi, T. Turnbull, S. Sebastian and I. Kempson, *Int. J. Mol. Sci.*, 2021, **22**, 12827.
42 S. Karim, S. Halder, S. Mukherjee, U. Debnath, A. K. Misra, K. Jana and D. Das, *ACS Appl. Mater. Interfaces*, 2023, **15**, 26442–26456.
43 A. Dutta, S. Halder, I. Bhaumik, U. Debnath, D. Dhara, A. K. Misra and K. Jana, *ACS Pharmacol. Transl. Sci.*, 2024, **7**, 195–211.
44 E. Eruslanov and S. Kusmartsev, *Methods Mol. Biol.*, 2010, **594**, 57–72.
45 M. Shit, S. Halder, A. Dey, B. Dutta, A. Chanthapally, K. Jana and C. Sinha, *Inorg. Chem.*, 2023, **62**, 19937–19947.
46 L. B. Sullivan, E. Martinez-Garcia, H. Nguyen, A. R. Mullen, E. Dufour, S. Sudarshan, J. D. Licht, R. J. Deberardinis and N. S. Chandel, *Mol. Cell*, 2013, **51**, 236–248.
47 J. Zielonka, J. Vasquez-Vivar and B. Kalyanaraman, *Nat. Protoc.*, 2008, **3**, 8–21.
48 G. Kroemer, L. Galluzzi and C. Brenner, *Physiol. Rev.*, 2007, **87**, 99–163.
49 R. Patra, S. Halder, R. Saha, K. Jana and K. Sarkar, *ACS Biomater. Sci. Eng.*, 2024, **10**, 2299–2323.
50 C. J. Aslakson and F. R. Miller, *Cancer Res.*, 1992, **52**, 1399–1405.
51 P. K. Parida, B. Mahata, A. Santra, S. Chakraborty, Z. Ghosh, S. Raha, A. K. Misra, K. Biswas and K. Jana, *Cell Death Dis.*, 2018, **9**, 448.